J. Phys. Chem. C, 119, 28970 (2015)

An Adsorption Study of CH_4 on ZSM-5, MOR, and ZSM-12 Zeolites

Yiwei Zhang,[1,2] JingYe Yu,[1] Yu-Hao Yeh,[1] Raymond. J. Gorte[1*], Srinivas Rangarajan[3], Manos Mavrikakis[3]

[1] Chemical and Biomolecular Engineering, University of Pennsylvania, 231 S. 34 Street, Philadelphia, PA 19104

[2] School of Chemistry and Chemical Engineering, Southeast University, Nanjing 211189, P.R.China

[3] Chemical and Biological Engineering, University of Wisconsin - Madison, Madison, WI 53706, USA.

Abstract

CH_4 adsorption was studied experimentally and theoretically on ZSM-5, MOR, and ZSM-12 zeolites using calorimetric measurements at 195 K and plane wave DFT calculations. Differential heats measured on four different H-ZSM-5 samples were determined to be 22.5±1 kJ/mol, independent of Brønsted site density or defect concentration. However, DFT calculations performed using various functionals and on the most stable Brønsted site indicated that CH_4 should bind to this site by an additional 1 to 7 kJ/mol, a discrepancy that is due to the inability of standard DFT methods to capture hydrogen-bonding effects accurately with CH_4. Differential heats for CH_4 in MOR were 30±1 kJ/mol at low coverages, falling to 25 kJ/mol for coverages above one molecule per 8-membered-ring side pocket, while differential heats on ZSM-12 were initially 22.5 kJ/mol, decreasing to 21 kJ/mol with coverage. DFT calculations on the siliceous form of the zeolites were able to predict these values within 5 kJ/mol in most cases. The results indicate that CH_4 is an excellent probe molecule for characterizing the pore structure of zeolites.

Introduction

Methane, the main component of natural gas, would be an attractive fuel for vehicles if it could be stored at high densities, without requiring high pressures or cryogenic temperatures. One method for achieving high storage densities at reasonable temperatures and pressures involves adsorbing methane on a porous solid and a great deal of effort has gone into developing both materials and theoretical understanding for this application[1,2]. Because adsorption of methane is physical in nature, adsorption isotherms and energetics depend in a rather simple manner on the composition of the solid adsorbent[3] and on the size and shape of the pores that make up the solid. Furthermore, since the theory for adsorption of methane is reasonably well developed, it is possible to predict what the adsorption properties of a crystalline material will be and what the best porous solid structures will be[4].

For similar reasons, it should be possible to use experimental data to characterize the nanopores in unknown or poorly crystalline materials. For example, the zero-coverage heats of adsorption for methane in siliceous zeolites with one-dimensional pores made up of 10-, 12-, and 14-membered rings (MR) (TON, MTW (also known as ZSM-12), and UTD-1) were reported to be 27.2, 20.9, and 14.2 kJ/mol, respectively[5]. If one knew that a particular siliceous material had cylindrical pores, the heats of adsorption could be used to estimate the pore size. Real zeolite structures have more complex pore structures and the concept of using the distribution of

adsorption energies could allow one to map the structure. A particularly interesting material for understanding the effect of structure on adsorption is the zeolite with the MOR structure. MOR has one-dimensional, 12-MR channels with 8 MR side pockets. MOR exhibits unique catalytic properties for the carbonylation of dimethyl ether[6], most likely because the 8-ring pockets are able to stabilize the intermediate structures.

One complication for determining pore structure from a distribution of adsorption energies is that most zeolites are not defect free or purely siliceous. Many zeolite structures, including MOR, are synthesized with framework Al and must have non-framework cations to balance the charge. The simplest charge-balancing cation is the proton, which leads to Brønsted acidity. Even simple, polar molecules (e.g. CO) will adsorb preferentially on these sites and give an added contribution to the heats[7]. With non-polar molecules, the situation is less clear. Interactions between molecular O_2 and Brønsted sites are reported to be negligible[7], but there is both experimental[8,9] and theoretical[10,11] evidence that adsorption on the Brønsted sites contributes to the heats of adsorption for small alkanes. Because adsorption energies have been shown to scale with proton affinities for both protonated and hydrogen-bonded adsorption complexes[12,13] and because methane has a much lower proton affinity compared to even ethane (543.5 kJ/mol versus 596.3 kJ/mol[14], the influence of acid sites on methane adsorption is not well known. There are a few reported studies of methane adsorption on H-ZSM-5[15–17], but the role of Brønsted sites in adsorption of methane has not been clearly demonstrated.

In order to measure the spectrum of adsorption energies in a material that has more than one type of site, it is essential that calorimetric measurements be performed at an appropriate temperature[18]. If the measurement temperature is too low so that adsorption is not reversible, the adsorbate will not be able to sample all possible sites. In this case, if adsorption is irreversible, each gas dose will saturate different parts of the sample, leading to differential heats of adsorption that are constant with coverage, even if the sites are not identical[19]. On the other hand, for weakly bound molecules like methane, adsorption should be performed at temperatures that are low enough for adsorption to occur preferentially at the strongest sites. For example, if a material has two types of sites (e.g. in MOR, these might be pocket sites and main-channel sites), separated in energy by values similar to $\boldsymbol{kT}$ (where $\boldsymbol{k}$ is the Boltzmann constant and $\boldsymbol{kT}$ ~2.5 kJ/mol at room temperature), a significant fraction of molecules added to a fresh sample will occupy the weaker sites at equilibrium, especially if the weaker sites are present in higher concentrations and if

adsorption on those sites is entropically preferred. Indeed, sample calculations have suggested that it is likely impossible to observe minority sites having a heat of adsorption that is 5 kJ/mol higher than that of the majority sites using differential calorimetry at room temperature[18].

Past work from one of our laboratories demonstrated that site heterogeneity in physisorption can be measured using differential calorimetry at 195 K[7]. In siliceous, defect-free ZSM-5 (a zeolite with the MFI structure), the differential heats of adsorption for CO were found to be 16±1 kJ/mol, independent of coverage. On the analogous acidic H-ZSM-5, the differential heats for CO adsorption were 10 kJ/mol higher at low coverages, falling to the same value as on the siliceous ZSM-5 at coverages above one CO per Brønsted site. Molecules such as O_2, which do not interact with Brønsted sites, showed the same heats of adsorption on both samples[20]. Therefore, the coverage-dependent differential heats provide a measure of the site energetics for these materials.

In the present work, we set out to determine whether differential calorimetry can be used to distinguish structural differences in similar zeolites, using MOR and MTW as the examples. Using both theoretical calculations and experimental measurements, we will show that methane adsorption at 195 K appears to be an excellent probe for determining structural differences. By studying CH_4 adsorption in a series of H-ZSM-5 samples, we show that the presence of Brønsted sites does not affect the heats of adsorption for CH_4.

Methods

Experimental

The Tian-Calvet calorimeter used in this study was home-built and has been described in detail elsewhere[17]. The instrument was constructed from five, 2.54-cm square, thermal-flux meters (International Thermal Instrument Company, Del Mar, CA) placed between a cubic, pyrex sample cell and a large Al block. The 1-g zeolite samples, pressed into wafers and placed at the bottom of the pyrex cube, were covered with quartz chips in order to prevent heats losses due to radiation out the top. The sample was evacuated using a mechanical pump and exposed to gases from a calibrated GC sample loop. All experiments were performed at 195 K, maintained by placing the Al-block heat sink in a styrofoam container with dry ice. The thermopiles had previously been calibrated by passing current through a Pt wire placed between the sample cell and the thermopiles. The uncertainty in our measurement of each point was ~ 2%, corresponding to ~0.5 kJ/mol;

however, the uncertainty in our calibration factor is larger, so that the uncertainty in the absolute values of the differential heats is ~1 kJ/mol.

The zeolites in this study, along with some of their properties, are listed in Table 1. Two of the H-ZSM-5 and the H-MOR samples are commercially available from Zeolyst. The two ZSM-5 samples, prepared at the University of Delaware, used fluoride-containing media to achieve low silanol defect concentrations[21] A typical synthesis was as follows: distilled water was mixed with Ludox AS-40 silica sol, tetrapropylammonium bromide (TPABr), NH4F, and A1$(NO_3)_3 \cdot 9H_2O$. (A purely siliceous ZSM-5 was prepared using the same procedure, but without the addition of A1$(NO_3)_3 \cdot 9H_2O$.) The mixture was heated at 450 K for seven days in a Teflon-lined autoclave. After filtering, the solid was calcined at 823 K in flowing dry air for 6 h. These samples were noticeably more hydrophobic and 2-propanamine molecules in excess of twice the Brønsted-site densities could be easily evacuated at room temperature, whereas the excess amine molecules in the commercial samples could only be removed by heating. The H-ZSM-12 sample was used in a previous study and has been described there in more detail[5]. Brønsted-site concentrations were determined using simultaneous temperature-programmed desorption and thermogravimetric analysis of 2-propanamine[22]. Pore volumes were determined from gravimetric uptakes of n-hexane at room temperature and 10 torr, assuming the pore volume becomes filled with liquid-like n-hexane.

Calculations

All electronic structure calculations were carried out using Vienna ab initio simulation package (VASP)[23,24]- a plane wave density functional theory (DFT) code. PAW[25] potentials with generalized gradient approximation (GGA) using the PBE exchange correlation functional[26] with Grimme-D2[27] semi-empirical dispersion corrections were used. The Brillouin zone was sampled using only the gamma point in view of the large supercell size. A Gaussian smearing of 0.1 eV was used and all energies were extrapolated to 0 K. A plane wave cutoff of 400 eV and density wave cutoff of 600 eV were used with a convergence criteria of all forces being smaller than 0.02 eV/Å. We refer to this level of theory as DFT-D2 in this work. The calculated (experimental[28] in parenthesis) lattice parameters for the three zeolites in their siliceous forms are: (a) 20.2 x 19.9 x 13.3 Å (20.1 x 19.7 x 13.1 Å) for the orthorhombic phase of ZSM-5, (b) 18.4 x 20.7 x 7.6 Å (18.3 x 20.5 x 7.5 Å) for the orthorhombic mordenite (MOR) structure, and (c) 25.8 x 5.3 x 12.2 Å (25.6

x 5.3 x 12.1 Å with β=109.3º for both) for zeolite ZSM-12 in the monoclinic form. In these calculations, the atoms of the zeolite were fixed at coordinates specified in the structural information published by IZA website All molecular adsorption calculations for ZSM-5 and MOR were performed in a supercell comprising one full periodic unit while those on ZSM-12 were carried out in a supercell that had two unit cells (two units in the y-axis); these cells enable us to explore low adsorbate coverages. All atoms were relaxed in these calculations and spin polarization was considered for the oxygen molecule in the gas and adsorbed phase. Gas phase calculations were carried out in the same level of theory as above in a cell of size 20 x 20.5 x 21 Å allowing for more than 10 Å of vacuum between periodic images. Figures of zeolite structures and adsorbate configurations were generated using VESTA[29].

The binding energy (BE) of an adsorbate molecule is calculated as:

$$\boldsymbol{BE = E_{molecule+Zeolite} - E_{molecule,\,gas} - E_{Zeolite}} \quad \textbf{(1)}$$

where $\boldsymbol{E_{molecule+Zeolite}}$ is the total energy of the zeolite with the adsorbed molecule, $\boldsymbol{E_{molecule,\,gas}}$ is the total energy of the gaseous molecule, and $\boldsymbol{E_{Zeolite}}$ is the total energy of the zeolite (catalyst). We report results on both Brønsted and non-Brønsted forms of multiple sites on the zeolite ZSM-5; for MOR and ZSM-12, only the non-Brønsted sites are considered. The calculation of $\boldsymbol{E_{molecule+Zeolite}}$ and $\boldsymbol{E_{Zeolite}}$ on a Brønsted site involved performing electronic structure calculations on a zeolite supercell with a single Si atom being replaced by an Al atom (and adding one H atom to a neighboring oxygen atom); for the corresponding non-Brønsted site, similar calculations were performed on its topologically identical site in a siliceous supercell.

Zero point energy (ZPE) corrections were included (unless otherwise stated) in all binding energy values reported here. The vibrational frequencies ν_i of the adsorbate (and the Brønsted proton, if present) were computed using harmonic approximation and ZPE was calculated using the following formula

$$\boldsymbol{ZPE = \frac{1}{2}\sum_{i=1}^{\#\,modes} h\nu_i} \quad \textbf{(2)}$$

Since there are multiple topologically identical locations in a zeolite supercell, we also performed sample calculations to test if the presence of a Brønsted site in a supercell affects adsorption on a topologically identical non-Brønsted site and compared this with the binding energy values on the siliceous supercell; we observed negligible (< 1 kJ/mol) differences in all cases.

Temperature corrections were added to the binding energy to get enthalpy of adsorption. This was done by calculating temperature-dependent entropy values for the adsorbate in the gas and adsorbed phases, fitting a polynomial (Shomate equations) to this data, calculating heat capacity from the resulting expression, and calculating a temperature contribution to the total energy. The details of this procedure are given in the supporting information (Method S1).

Results and Discussion

H-ZSM-5

Experimental

In order to understand the possible effects of Brønsted sites and silanol defects on CH_4 adsorption, calorimetric measurements were performed at 195 K on the four H-ZSM-5 samples listed in Table 1. The differential heats are reported as a function of coverage in Figure 1, with results for the two Zeolyst samples in Figure 1a) and for the two defect-free samples in Figure 1b). Within experimental uncertainty, the heats of adsorption at coverages below 0.6 mmol/g were independent of coverage on all of the samples. The differential heats were 22.5±1 kJ/mol on the two Zeolyst samples and 22±1 on the two defect-free samples. The Brønsted-site densities on these samples ranged from 0.010 mmol/g to 0.47 mmol/g, implying that interactions with the Brønsted sites were too small to observe in calorimetry. The very small difference between the results on the defect-free samples and the Zeolyst samples were less than the experimental uncertainty.

Interestingly, the equilibrium constants, determined from the slope of the isotherm near zero coverage and reported in Table 2, were not identical on the four samples. The values for the four samples differed by a factor of about 4, with H-ZSM-5(50) showing the highest value and ZSM-5(F,Si) the lowest. There is a strong correlation between the equilibrium constant and the Brønsted-site density but there does not appear to be any dependence on whether or not the samples are defect-free. If the change in equilibrium constant were simply due to enthalpic interactions with the Brønsted sites, the factor of 4 at 195 K would imply that the heats of adsorption should be 2.2 kJ/mol higher on H-ZSM-5(50) compared to ZSM-5(F,Si). This is significantly higher than the uncertainty in the calorimetric measurements, implying that there may be some entropic effects associated with adsorption near the Brønsted sites.

For example, since adsorbed CH_4 is likely very mobile, we suggest that the effect of the Brønsted sites might be to reduce this mobility. The change in adsorption entropy associated with

a factor of 4 change in equilibrium constant is 11.5 J/mol·K at 195 K. If Brønsted sites were to reduce the mobility from something like a two-dimensional to a one-dimensional gas, the partition functions could be calculated using Equations (3) and (4):

$$S_{trans,2D} = R\left[\ln\left(\frac{2\pi mkT}{h^2}\right) + ln\left(\frac{SA}{N}\right) + 2\right] \quad (3)$$

$$S_{trans,1D} = R\left(\log\left(\frac{\sqrt{2\pi mkT}}{h}\right) + \log(L_0) + 1.5\right) \quad (4)$$

where m is the mass of the molecule, k is the Boltzmann constant, and h Planck's constant. $\frac{SA}{N}$ is the average surface area available for a molecule at the reference state of a monolayer coverage, equal to 200 pm x 600 pm for ZSM-5[11], and L_0 can be taken to be a lattice parameter, on the order of 600 pm in this case. For CH_4 at 195 K, the difference between these values is nearly 20 J/mol·K.

Calculations

Since previous theoretical studies have indicated hydrocarbons should interact with Brønsted sites[16,30], we performed theoretical studies on H-ZSM-5 to understand what effect Brønsted sites might have on the adsorption of simple molecules. In addition to examining the adsorption of CH_4, we also examined adsorption of CO on H-ZSM-5, since previous measurements indicated that CO adsorbs on Brønsted sites with an additional 10 kJ/mol (This result was repeated here for the H-ZSM-5(F,Al) sample, with data shown in Figure S1)[7].

Two locations for the acid sites were considered. The most stable acid site (Al7-O17-Si8 defined per the scheme adopted by IZA) is shown in Figure S2, where the Brønsted proton (bonded to O17) is hydrogen bonded to another oxygen atom (O-H distance of 1.85 Å). A less stable site (Si12-O26-Al12) (by 0.23 eV or ~22 kJ/mol) was also considered at the entrance of the sinusoidal channel and pointing into the straight channel is shown in Figure S3. These two sites have been considered in the literature as the likely positions for the Brønsted sites in HZSM-5[31–34]. The enthalpy of adsorption at the DFT-D2 level of theory for CO and CH_4 on these two locations, with and without the Brønsted site, are reported in Table 3 and discussed below. The corresponding binding energy values (ZPE corrected) are in Table S1. Figures S4-S7 show the adsorption structures for CH_4 and CO on the Brønsted and non-Brønsted forms of the two sites considered.

CO binds via the carbon atom on both Brønsted and non-Brønsted sites of ZSM-5 similar to the observations made in computational studies of other proton-form zeolites[35,36]; in the

presence of a Brønsted site, the molecule points towards the Brønsted proton, leading to an additional stabilization of about 7 kJ/mol for T7-O17-T8 and 22 kJ/mol eV for the T12-O26-T12 site. The adsorption enthalpy values (-26.7 kJ/mol) on the most stable Brønsted acid site (T7-O17-T18) match remarkably well with the microcalorimetric data (26.5 kJ/mol) for carbon monoxide on ZSM-5[20]. On the other hand, the binding energy on the Brønsted site of T12-O26-T12 is about 14 kJ/mol higher than that of T7-O17-T8.

The calculated adsorption enthalpies of CH_4 on the Brønsted (-23.2 kJ/mol) and siliceous forms -21.2 kJ/mol) of the T7-O17-T8 site are close to experimental values (~22 kJ/mol); however, DFT-D2 calculations show an effect of the Brønsted site of about 2 kJ/mol. The binding energy on the Brønsted site of T12-O26-T12 is about 12 kJ/mol larger than that on T7-O17-T8, leading again to a more pronounced effect of the Brønsted site at the T12-O26-T12 location. It should be noted that the lower effect of hydrogen bonding for the T7-O17-T8 site is potentially due to stabilization of the Brønsted hydrogen atom through hydrogen bonding (Figure S2). Recently, Tuma and Sauer adopted a hybrid MP2: DFT method to calculate the binding energy and proton transfer barriers of methane on a number of proton-form zeolites[37]. This higher level of theory can be used to benchmark our results. The authors report a ZPE-corrected binding energy value of -28.5 kJ/mol on the T7-O17 site (although named T7-O7 according to their naming convention) compared to our -26 kJ/mol (see Table S1). In addition, we performed additional calculations on the T12 site studied by Tuma and Sauer (T12-O20 in their naming convention and T12-O8 in ours); the ZPE-correted binding energy values of methane adsorption on this site was found to be -29.9 kJ/mol, in close agreement with the published value of -30.1 kJ/mol (see Table S2). The effect of Brønsted site for methane adsorption on the T12-O8 site is about 3.5 kJ/mol.

Because experimental data suggests acid sites have a negligible effect on CH_4 adsorption enthalpies, we investigated the origin of this DFT-predicted effect by considering other exchange correlation functionals, as well as alternative treatments of dispersion effects. Table 4 lists the different levels of theory considered in this study, and the corresponding calculated difference in the binding energy values (not ZPE corrected) of CH_4 on the Brønsted and non-Brønsted forms of the T7-O17-T8 site. The difference values are between 0.01 and 0.07 eV (~1 to 7 kJ/mol) in all cases and arise primarily due to the choice of the exchange correlation functional used in the calculations. Similar observations can be made for the T12-O26-T12 site as well (see Table S3). These results are consistent with other theoretical studies[16,30] but do not agree with the

experimental observations. We suggest the discrepancy between theory and experiment in this case is due to the inability of standard DFT methods to capture hydrogen-bonding effects accurately. Various benchmarking studies on the accuracy of DFT functionals to treat hydrogen bonding have been reported[44–47]. While the specific conclusions of these studies vary (some report under-prediction while others observed over-prediction with respect to a higher level of theory such as coupled cluster calculations) and the reference set of molecules considered are different, they all point to intrinsic errors in standard generalized gradient-corrected exchange correlation functionals in treating hydrogen bonding, in line with our observations. In view of our experimental data, the Brønsted sites will not be considered further in our calculations.

MOR and MTW

Experimental Data

In order to determine the effect of zeolite structure on adsorption properties, we performed calorimetric measurements of CH_4, O_2, and Ar on MOR and ZSM-12. As discussed in the Introduction, the main channels in both MOR and ZSM-12 are 12 MR. However, MOR also has 8-MR pockets on the sides. Although the volume of these pockets is small compared to that of the main channels, the corrugation that results from the openings to the side pockets causes the pore surfaces to be rougher on the molecular scale. As with CH_4, O_2 and Ar are not expected to interact with Brønsted sites, so that most of the interactions should be due to dispersion forces with the siliceous walls[20].

Figure 2 shows the differential heats for CH_4 on ZSM-12 and MOR. On ZSM-12, the differential heats are reasonably constant, starting at 23.0 kJ/mol at zero coverage and decreasing slightly to 21.5 kJ/mol at 0.4 mmol/g. In a previous calorimetric study carried out at room temperature, the differential heats also decreased slightly with coverage but the reported heats were about 2 kJ/mol lower[5]. About 1.2 kJ/mol of this difference can be explained by the heat of adsorption changing with temperature. This value was determined by assuming CH_4 loses its translational degrees of freedom in going to the adsorbed phase, so that the heat capacities of gas-phase and adsorbed-phase CH_4 change by (3/2)R. In any case, the numbers here are probably more accurate than those reported previously due to the fact that lower gas pressures were required to obtain a given coverage at 195 K. Although ZSM-12 consists of 12-MR channels, the differential

heats are very close to that found on the 10-MR zeolite, ZSM-5. This is due to the fact that the intersecting channels in ZSM-5 make the channels effectively larger.

The heats of adsorption for CH_4 on MOR were significantly higher than those on MTW. At low coverages, the differential heats in MOR were almost 30 kJ/mol. For coverages between 0.25 and 0.45 mmol/g, the differential heats fell to 25 kJ/mol, then remained constant at that value. The higher heats are almost certainly associated with the 8-MR side pockets. While there are no simple, one-dimensional zeolites with 8-MR channels, it is noteworthy that the zero-coverage differential heats were only about 27 kJ/mol on the 10-MR, one-dimensional zeolite, TON. Furthermore, the coverage at which the differential heats fall on MOR is close to the side-pocket concentration of 0.35 mmol/g. The fact that there is no sharp demarcation at 0.35 mmol/g is due to the adsorption energies for molecules in the side pockets and in the corrugated main channels differing by a relatively small amount, so that both sites are being occupied simultaneously at 195 K, as discussed in the Introduction[18].

Figure 3 shows the corresponding differential heats for O_2 in the ZSM-12 and MOR samples. Heats of adsorption for O_2 in ZSM-12 were 16 kJ/mol, independent of coverage. As with CH_4, this value is again similar to the heat of adsorption reported for O_2 in siliceous ZSM-5[20]. The differential heats for O_2 on MOR, 20 kJ/mol, were higher than those found on ZSM-12; however, unlike the case for CH_4, the differential heats for O_2 were independent of coverage. Because O_2 should be able to fit in the 8-ring side pockets, we suggest that difference in adsorption enthalpies between the side pockets and the main channels is similar or less than $\boldsymbol{kT}$, so that both sites fill simultaneously. The results for Ar in MOR and ZSM-12, shown in Figure 4, are nearly the same as those for O_2.

Calculations

The adsorption of CH_4, O_2, and Ar in siliceous MOR and ZSM-12 was studied using DFT-D2. Figure S8 shows a schematic of MOR. Molecules can adsorb in the 12-MR channel and the 8-MR side pocket. While MOR also has an 8-MR channel as marked in Figure S8, the dimension of its minor axis (4.3 Å) prevents adsorption in this region; we did not observe strong adsorption in the 8 MR channels except for a few less stable structures at the intersection of 8 MR channels and 8 MR side pockets. The 12 MR channel close to the walls (marked region II) and the region of 8 MR side pockets (marked region II) are potential locations for adsorption.

The calculated adsorption enthalpy of CH_4, O_2, and Ar in the two regions of MOR are given in Table 3 (ZPE corrected binding energies are in Table S4) and their adsorption structures are shown in Figure 5. CH_4 binding energies vary from ~ -28 kJ/mol to -17 kJ/mol) while O_2 and Ar binding energy variations are smaller. In all cases, DFT-D2 predicts a higher binding energy for the side pockets than the straight channels. Further, the DFT-D2 binding energy in the 8-MR side pockets match experimental heats at low coverage, corroborating our argument that the side pockets get filled first. DFT-D2 under-predicts the binding energy of CH_4 in the 12 MR channel by 5 kJ/mol (compared to experimental heats at high coverage). This under-prediction appears to be uniform for all three adsorbates because accounting for this brings DFT-D2 predictions to within 2 kJ/mol of experimental heats at high coverages for O_2 and Ar. This uniform deviation probably arises from intrinsic error in the variation of the dispersion potential as a function of distance of the adsorbate from the wall. The trends from DFT-D2, however, suggest that the heats of adsorption of O_2 and Ar are independent of the coverage because the difference between the adsorption enthalpies of the side pockets and the main channel is small compared to $\boldsymbol{kT}$.

A schematic of ZSM-12 showing the 12-MR channels is given in Figure S9. The DFT-D2 adsorption enthalpy of CH_4, O_2, and Ar in ZSM-12 is given in Table 4 (ZPE corrected binding energy values are in Table S5) and the adsorption structures are shown in Figure 6. CH_4 (-20.3 kJ/mol) binds more strongly than O_2 (-13.8 kJ/mol) and Ar (-16.6 kJ/mol), similar to what was found in MOR; these are within 4 kJ/mol of the experimental differential heats. The binding energy of CH_4 in ZSM-12 is within 1 kJ/mol of that on ZSM-5 in agreement with the experiments. Clearly, comparing the three zeolites, the binding energy of adsorbates is higher in confined spaces of the zeolite (such as the side pockets of MOR) due to increased dispersion interactions. Overall, the calculations confirm our initial proposition and experimental results that a probe molecule that interacts with the zeolite purely through dispersion interactions (such as methane) can be used to characterize the pore geometry of zeolites.

Conclusions

Experimental differential heats of adsorption for CH_4 depend strongly on the solid nanostructure but not on the presence of Brønsted sites, implying that calorimetric measurements

at 195 K could be used to probe the nanostructure of unknown materials. The comparison of the experimental results with DFT demonstrated that the theory accurately describes the effect of zeolite structure on CH_4 adsorption but over-predicts the effect of Brønsted sites.

Acknowledgements

J-YY, Y-HY, and RJG acknowledge support from the Catalysis Center for Energy Innovation, an Energy Frontier Research Center funded by the U.S. Department of Energy, Office of Science, Office of Basic Energy Sciences under Award number DE-SC0001004. YZ acknowledges support from the National Natural Science Foundation of China (Grant No. 21376051), Natural Science Foundation of Jiangsu Province of China (Grant No. BK20131288) and the Fundamental Research Funds for the Central Universities (3207045421). SR and MM acknowledge support from the Air Force Office of Scientific Research under a Basic Research Initiative grant (AFSOR FA9550-12-1-0481). The computational work was performed partly using supercomputing resources at EMSL, a National scientific user facility at Pacific Northwest National Lab (PNNL), the Center for Nanoscale Materials (CNM) at Argonne National Lab (ANL), and the National Energy Research Scientific Computing Center (NERSC). EMSL is sponsored by the Department of Energy's Office of Biological and Environmental Research located at PNNL. CNM and NERSC are supported by the U.S. Department of Energy, Office of Science, under contracts DE-AC02-06CH11357 and DE-AC02-05CH11231, respectively. This research was also partially performed using the compute resources and assistance of the UW-Madison Center For High Throughput Computing (CHTC) in the Department of Computer Sciences. The CHTC is supported by UW-Madison, the Advanced Computing Initiative, the Wisconsin Alumni Research Foundation, the Wisconsin Institutes for Discovery, and the National Science Foundation, and is an active member of the Open Science Grid, which is supported by the National Science Foundation and the U.S. Department of Energy's Office of Science. The assistance of Prof Raul Lobo and Dr. Eyas Mahmoud in the preparation of zeolite samples is gratefully acknowledged.

Literature cited

(1) Zhang, H.; Deria, P.; Farha, O. K.; Hupp, J. T.; Snurr, R. Q. A Thermodynamic Tank Model for Studying the Effect of Higher Hydrocarbons on Natural Gas Storage in Metal–organic Frameworks. *Energy Env. Sci* **2015**, *8* (5), 1501–1510.

(2) Getman, R. B.; Bae, Y.-S.; Wilmer, C. E.; Snurr, R. Q. Review and Analysis of Molecular Simulations of Methane, Hydrogen, and Acetylene Storage in Metal–Organic Frameworks. *Chem. Rev.* **2012**, *112* (2), 703–723.

(3) Koh, H. S.; Rana, M. K.; Wong-Foy, A. G.; Siegel, D. J. Predicting Methane Storage in Open-Metal-Site Metal–Organic Frameworks. *J. Phys. Chem. C* **2015**, *119* (24), 13451–13458.

(4) Simon, C. M.; Kim, J.; Gomez-Gualdron, D. A.; Camp, J. S.; Chung, Y. G.; Martin, R. L.; Mercado, R.; Deem, M. W.; Gunter, D.; Haranczyk, M.; et al. The Materials Genome in Action: Identifying the Performance Limits for Methane Storage. *Energy Env. Sci* **2015**, *8* (4), 1190–1199.

(5) Savitz, S.; Siperstein, F.; Gorte, R. J.; Myers, A. L. Calorimetric Study of Adsorption of Alkanes in High-Silica Zeolites. *J. Phys. Chem. B* **1998**, *102* (35), 6865–6872.

(6) Cheung, P.; Bhan, A.; Sunley, G. J.; Iglesia, E. Selective Carbonylation of Dimethyl Ether to Methyl Acetate Catalyzed by Acidic Zeolites. *Angew. Chem. Int. Ed.* **2006**, *45* (10), 1617–1620.

(7) Savitz, S.; Myers, A. L.; Gorte, R. J. Calorimetric Investigation of CO and N2 for Characterization of Acidity in Zeolite H−MFI. *J. Phys. Chem. B* **1999**, *103* (18), 3687–3690.

(8) Ramachandran, C.; Williams, B.; Vanbokhoven, J.; Miller, J. Observation of a Compensation Relation for N-Hexane Adsorption in Zeolites with Different Structures: Implications for Catalytic Activity. *J. Catal.* **2005**, *233* (1), 100–108.

(9) Eder, F.; Lercher, J. A. Alkane Sorption in Molecular Sieves: The Contribution of Ordering, Intermolecular Interactions, and Sorption on Brønsted Acid Sites. *Zeolites* **1997**, *18* (1), 75–81.

(10) Bučko, T.; Hafner, J. The Role of Spatial Constraints and Entropy in the Adsorption and Transformation of Hydrocarbons Catalyzed by Zeolites. *J. Catal.* **2015**, *329*, 32–48.

(11) De Moor, B. A.; Reyniers, M.-F.; Gobin, O. C.; Lercher, J. A.; Marin, G. B. Adsorption of C2−C8 N -Alkanes in Zeolites. *J. Phys. Chem. C* **2011**, *115* (4), 1204–1219.

(12) Parrillo, D. J.; Gorte, R. J. Characterization of Acidity in H-ZSM-5, H-ZSM-12, H-Mordenite, and HY Using Microcalorimetry. *J. Phys. Chem.* **1993**, *97* (34), 8786–8792.

(13) Lee, C.-C.; Gorte, R. J.; Farneth, W. E. Calorimetric Study of Alcohol and Nitrile Adsorption Complexes in H-ZSM-5. *J. Phys. Chem. B* **1997**, *101* (19), 3811–3817.

(14) Hunter, E. P.; Lias, S. G. Evaluated Gas Phase Basicities and Proton Affinities of Molecules: An Update. *J. Phys. Chem. Ref. Data* **1998**, *27* (3), 413–656.

(15) Papp, H.; Hinsen, W.; Do, N.; Baerns, M. The Adsorption of Methane on H-ZSM-5 Zeolite. *Thermochim. Acta* **1984**, *82* (1), 137–148.

(16) Piccini, G.; Alessio, M.; Sauer, J.; Zhi, Y.; Liu, Y.; Kolvenbach, R.; Jentys, A.; Lercher, J. A. Accurate Adsorption Thermodynamics of Small Alkanes in Zeolites. Ab Initio Theory and Experiment for H-Chabazite. *J. Phys. Chem. C* **2015**, *119* (11), 6128–6137.

(17) Dunne, J.; Mariwala, R.; Rao, M.; Sircar, S.; Gorte, R.; Myers, A. Calorimetric Heats of Adsorption and Adsorption Isotherms. 1. O2, N2, Ar, CO2, CH4, C2H6, and SF6 on Silicalite. *Langmuir* **1996**, *12* (24), 5888–5895.

(18) Parrillo, D. J.; Gorte, R. J. Design Parameters for the Construction and Operation of Heat-Flow Calorimeters. *Thermochim. Acta* **1998**, *312* (1), 125–132.

(19) Parrillo, D.; Lee, C.; Gorte, R. Heats of Adsorption for Ammonia and Pyridine in H-ZSM-5: Evidence for Identical Brønsted-Acid Sites. *Appl. Catal. Gen.* **1994**, *110* (1), 67–74.

(20) Savitz, S.; Myers, A. L.; Gorte, R. J. A Calorimetric Investigation of CO, N2, and O2 in Alkali-Exchanged MFI. *Microporous Mesoporous Mater.* **2000**, *37* (1), 33–40.

(21) Axon, S. A.; Klinowski, J. Synthesis and Characterization of Defect-Free Crystals of MFI-Type Zeolites. *Appl. Catal. Gen.* **1992**, *81* (1), 27–34.
(22) Gorte, R. J. What Do We Know about the Acidity of Solid Acids? *Catal. Lett.* **1999**, *62* (1), 1–13.
(23) Kresse, G.; Furthmüller, J. Efficiency of Ab-Initio Total Energy Calculations for Metals and Semiconductors Using a Plane-Wave Basis Set. *Comput. Mater. Sci.* **1996**, *6* (1), 15–50.
(24) Kresse, G.; Furthmüller, J. Efficient Iterative Schemes for Ab Initio Total-Energy Calculations Using a Plane-Wave Basis Set. *Phys. Rev. B* **1996**, *54* (16), 11169.
(25) Kresse, G.; Joubert, D. From Ultrasoft Pseudopotentials to the Projector Augmented-Wave Method. *Phys. Rev. B* **1999**, *59* (3), 1758.
(26) Perdew, J. P.; Burke, K.; Ernzerhof, M. Generalized Gradient Approximation Made Simple. *Phys. Rev. Lett.* **1996**, *77* (18), 3865.
(27) Grimme, S. Semiempirical GGA-Type Density Functional Constructed with a Long-Range Dispersion Correction. *J. Comput. Chem.* **2006**, *27* (15), 1787–1799.
(28) Baerlocher, C.; McCusker, L. B.; Olson, D. H. *Atlas of Zeolite Framework Types*; Elsevier, 2007.
(29) Momma, K.; Izumi, F. VESTA 3 for Three-Dimensional Visualization of Crystal, Volumetric and Morphology Data. *J. Appl. Crystallogr.* **2011**, *44* (6), 1272–1276.
(30) Göltl, F.; Grüneis, A.; Bučko, T.; Hafner, J. Van Der Waals Interactions between Hydrocarbon Molecules and Zeolites: Periodic Calculations at Different Levels of Theory, from Density Functional Theory to the Random Phase Approximation and Møller-Plesset Perturbation Theory. *J. Chem. Phys.* **2012**, *137* (11), 114111.
(31) Ghorbanpour, A.; Rimer, J. D.; Grabow, L. C. Periodic, vdW-Corrected Density Functional Theory Investigation of the Effect of Al Siting in H-ZSM-5 on Chemisorption Properties and Site-Specific Acidity. *Catal. Commun.* **2014**, *52*, 98–102.
(32) Brändle, M.; Sauer, J. Acidity Differences between Inorganic Solids Induced by Their Framework Structure. A Combined Quantum Mechanics/molecular Mechanics Ab Initio Study on Zeolites. *J. Am. Chem. Soc.* **1998**, *120* (7), 1556–1570.
(33) Joshi, Y.; Thomson, K. Embedded Cluster (QM/MM) Investigation of C6 Diene Cyclization in HZSM-5. *J. Catal.* **2005**, *230* (2), 440–463.
(34) Mazar, M. N.; Al-Hashimi, S.; Cococcioni, M.; Bhan, A. β-Scission of Olefins on Acidic Zeolites: A Periodic PBE-D Study in H-ZSM-5. *J. Phys. Chem. C* **2013**, *117* (45), 23609–23620.
(35) Bučko, T.; Hafner, J.; Benco, L. Adsorption and Vibrational Spectroscopy of CO on Mordenite: Ab Initio Density-Functional Study. *J. Phys. Chem. B* **2005**, *109* (15), 7345–7357.
(36) Dominguez-Soria, V. D.; Calaminici, P.; Goursot, A. Theoretical Study of Host−Guest Interactions in the Large and Small Cavities of MOR Zeolite Models. *J. Phys. Chem. C* **2011**, *115* (14), 6508–6512.
(37) Tuma, C.; Sauer, J. Quantum Chemical Ab Initio Prediction of Proton Exchange Barriers between CH4 and Different H-Zeolites. *J. Chem. Phys.* **2015**, *143* (10), 102810.
(38) Perdew, J. P.; Chevary, J.; Vosko, S.; Jackson, K. A.; Pederson, M. R.; Singh, D.; Fiolhais, C. Erratum: Atoms, Molecules, Solids, and Surfaces: Applications of the Generalized Gradient Approximation for Exchange and Correlation. *Phys. Rev. B* **1993**, *48* (7), 4978.
(39) Perdew, J. P.; Chevary, J. A.; Vosko, S. H.; Jackson, K. A.; Pederson, M. R.; Singh, D. J.; Fiolhais, C. Atoms, Molecules, Solids, and Surfaces: Applications of the Generalized Gradient Approximation for Exchange and Correlation. *Phys. Rev. B* **1992**, *46* (11), 6671.
(40) Hammer, B.; Hansen, L. B.; Nørskov, J. K. Improved Adsorption Energetics within Density-Functional Theory Using Revised Perdew-Burke-Ernzerhof Functionals. *Phys. Rev. B* **1999**, *59* (11), 7413.
(41) Grimme, S.; Antony, J.; Ehrlich, S.; Krieg, H. A Consistent and Accurate Ab Initio Parametrization of Density Functional Dispersion Correction (DFT-D) for the 94 Elements H-Pu. *J. Chem. Phys.* **2010**, *132* (15), 154104.

(42) Perdew, J. P.; Ruzsinszky, A.; Csonka, G. I.; Vydrov, O. A.; Scuseria, G. E.; Constantin, L. A.; Zhou, X.; Burke, K. Restoring the Density-Gradient Expansion for Exchange in Solids and Surfaces. *Phys. Rev. Lett.* **2008**, *100* (13).
(43) Wellendorff, J.; Lundgaard, K. T.; Møgelhøj, A.; Petzold, V.; Landis, D. D.; Nørskov, J. K.; Bligaard, T.; Jacobsen, K. W. Density Functionals for Surface Science: Exchange-Correlation Model Development with Bayesian Error Estimation. *Phys. Rev. B* **2012**, *85* (23).
(44) Ireta, J.; Neugebauer, J.; Scheffler, M. On the Accuracy of DFT for Describing Hydrogen Bonds: Dependence on the Bond Directionality. *J. Phys. Chem. A* **2004**, *108* (26), 5692–5698.
(45) DiLabio, G. A.; Johnson, E. R.; Otero-de-la-Roza, A. Performance of Conventional and Dispersion-Corrected Density-Functional Theory Methods for Hydrogen Bonding Interaction Energies. *Phys. Chem. Chem. Phys.* **2013**, *15* (31), 12821.
(46) Boese, A. D. Density Functional Theory and Hydrogen Bonds: Are We There Yet? *ChemPhysChem* **2015**, *16* (5), 978–985.
(47) Rao, L.; Ke, H.; Fu, G.; Xu, X.; Yan, Y. Performance of Several Density Functional Theory Methods on Describing Hydrogen-Bond Interactions. *J. Chem. Theory Comput.* **2009**, *5* (1), 86–96.

Table 1. Zeolite samples used in this study.

Zeolite	Si/Al_2	Brønsted-acid site densities (μmol/g)	Pore volume with n-hexane (cm^3/g)
Zeolyst, H-ZSM-5(50)	50	470	0.1856
Zeolyst, H-ZSM-5(280)	280	80	0.1875
Defect free, H-ZSM-5(F,Al)	-	240	0.1744
Defect free, ZSM-5(F,Si)	-	10	0.1696
H-MOR	20	-	0.1026
ZSM-12	-	20	0.0939

Table 2. Equilibrium constants for adsorption of CH_4 on the four H-ZSM-5 samples at 195 K, determined from the slope of the isotherms near zero coverage.

Zeolite	Slope at zero coverage 10^{-7} (mol/(g*Pa))
H-ZSM-5(50)	6.47
H-ZSM-5(280)	4.15
H-ZSM-5(F,Al)	4.80
ZSM-5(F,Si)	1.54

Table 3: Calculated enthalpy of adsorption for CO and CH_4 (in kJ/mol) on Brønsted and non-Brønsted forms of two sites in ZSM-5 at 195 K.

Adsorbate	T7-O17-T8[a]		T12-O26-T12[a]	
	Brønsted[b]	Non-Brønsted[b]	Brønsted[b]	Non-Brønsted[b]
CO	-26.7	-19.1	-41.7	-19.6
Methane	-23.2	-21.2	-35.0	-20.1

[a] "T" refers to the tetrahedral atom that is either Si or Al atom; [b] "Brønsted" refers to adsorption on a Brønsted site formed by replacing a Si atom of Tx-Oy-Tz site by Al atoms and adding a hydrogen to the oxygen atom "y". For T7-O17-T8, Al replaces a Si atom in the tetrahedral position 7 and for T12-O24-T12 Al replaces Si atom in the tetrahedral position 12.

Table 4: Difference in CH_4 binding energies between Brønsted and non-Brønsted T7-O17-T8 site of ZSM-5 using different functionals and dispersion treatments

Method	Dispersion-corrected	Difference [eV (kJ/mol)][a,b]
Reference (PBE+D2)[26-27]	Yes	0.05 (4.7)
PBE[26]	No	0.05 (4.7)
PW91[38-39]	No	0.05 (4.9)
RPBE[40]	No	0.01 (1.3)
PBE[26] + D3[41]	Yes	0.07 (6.6)
PBEsol[42]	No	0.07 (6.5)
BEEF-vdW[43]	Yes	0.06 +/- 0.03[c] (6.0 +/- 2.9)

[a]positive value of the difference indicates CH_4 binds more strongly on the Brønsted site. [b]energy values are non-ZPE corrected. [c]estimated Bayesian statistical error calculated from a distribution of total energies estimated using an ensemble of parameter values representing the functional.

Table 5: Enthalpy of adsorption of CH_4, O_2, and Ar in the two adsorption regions of MOR at 195 K. All values are in kJ/mol.

Adsorbate	12 MR channel	8 MR side pocket
CH_4	-17.0	-27.5
O_2	-14.7	-19.9
Ar	-14.0	-20.6

Table 6: Enthalpy of adsorption of CH_4, O_2, and Ar in ZSM-12 at 195 K. All energy values are in kJ/mol.

Adsorbate	Binding energy
CH_4	-20.3
O_2	-13.8
Ar	-16.6

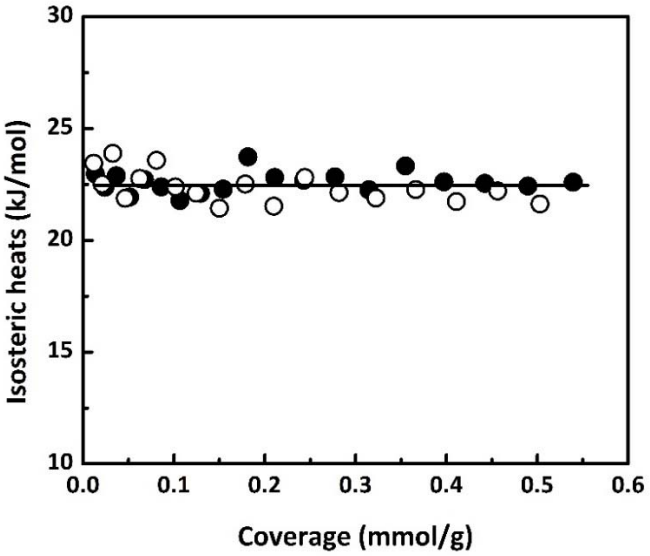

(a)

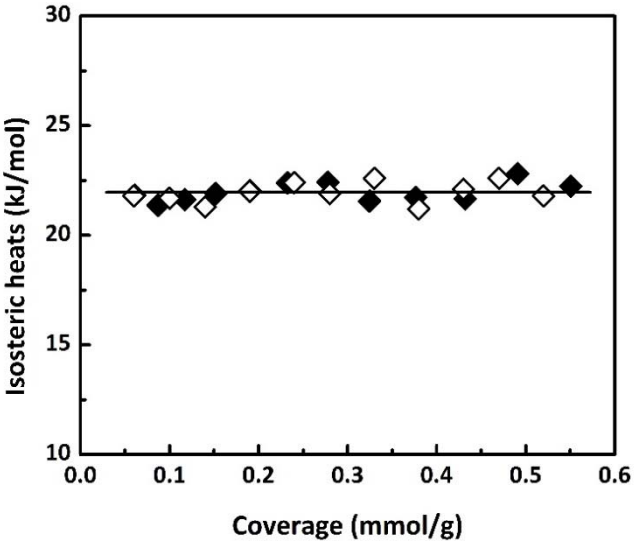

(b)

Figure 1. Differential heats for CH_4 adsorption on the different H-ZSM-5 samples at 195 K. (a) (●)H-ZSM-5(50) and (○)H-ZSM-5(280). (b) (◆) ZSM-5(F,Si) and (◇)H-ZSM-5(F,Al).

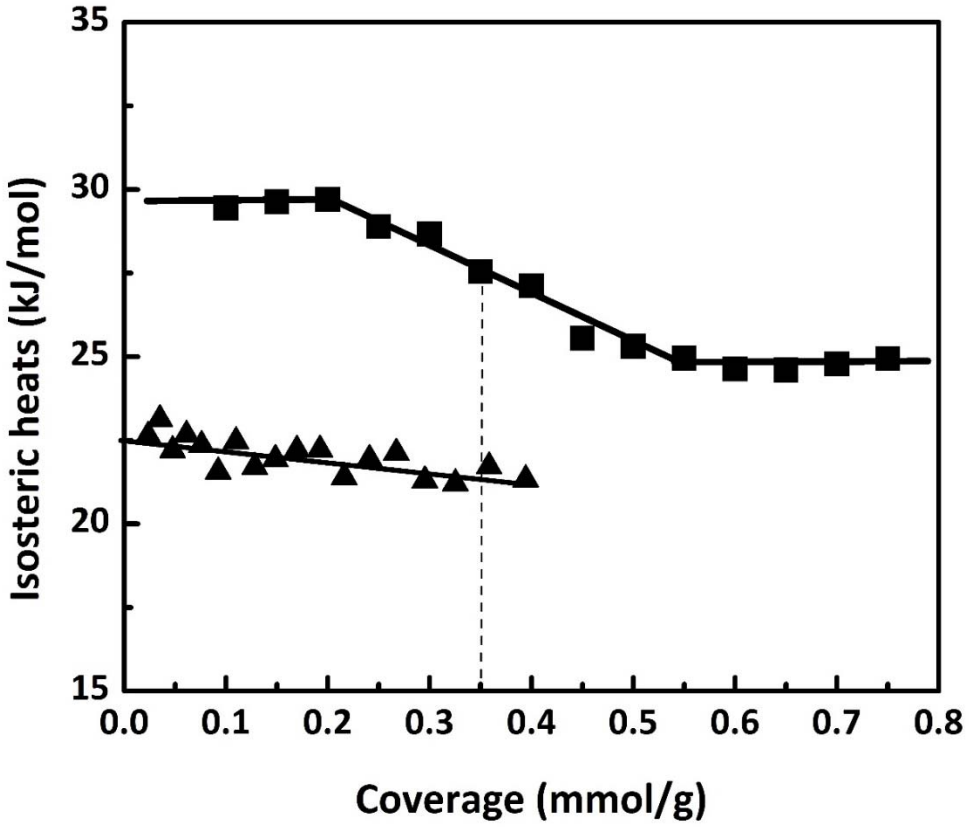

Figure 2. Differential heats of adsorption for CH_4 at 195 K on (■) H-MOR and (▲)H-ZSM-12.

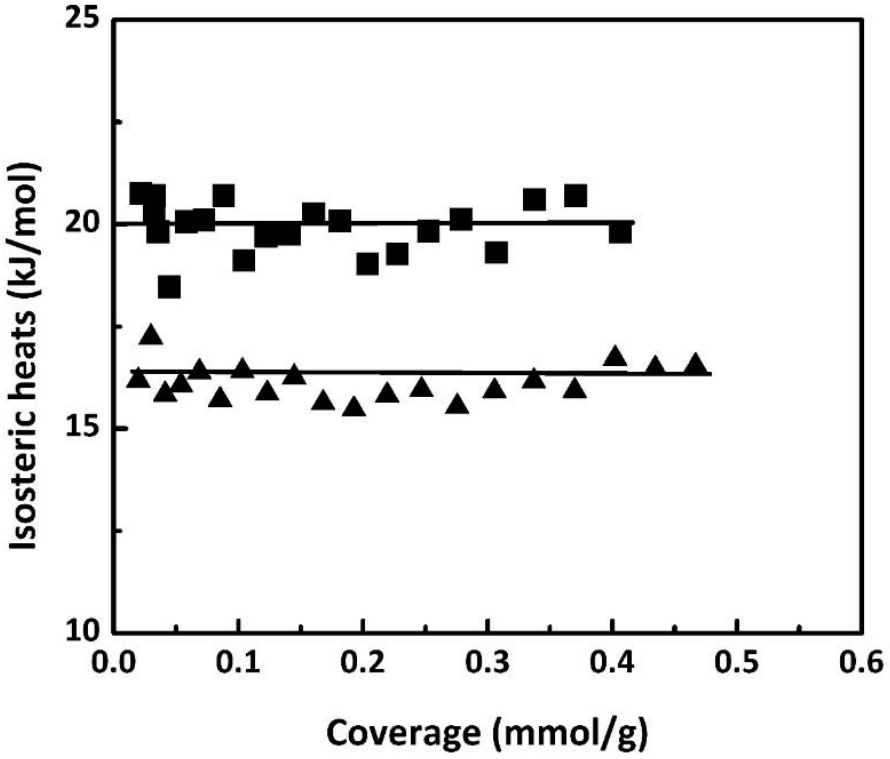

Figure 3. Differential heats of adsorption for O_2 at 195 K on (■) H-MOR and (▲) H-ZSM-12.

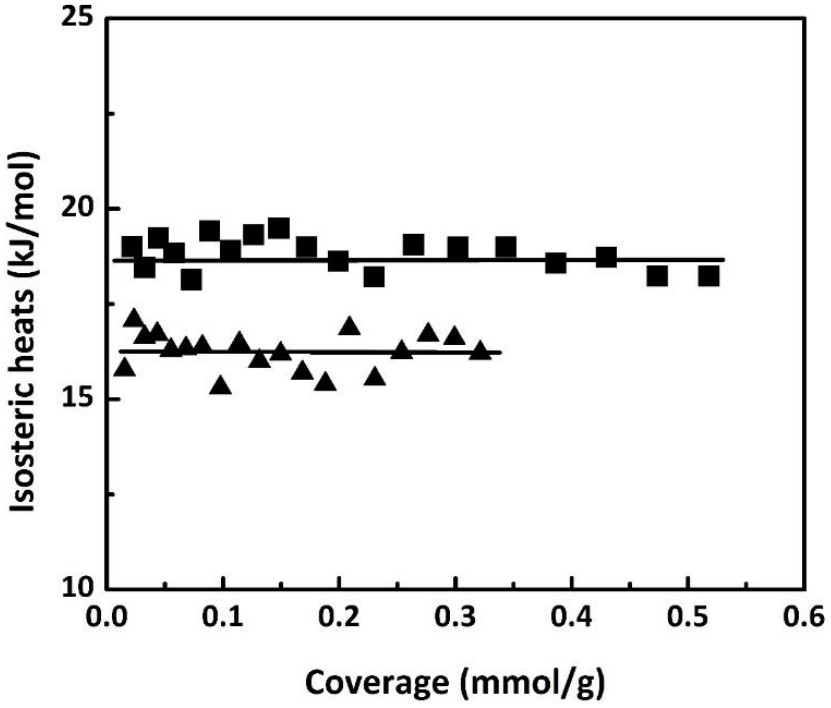

Figure 4. Differential heats of adsorption for Ar at 195 K on (■) H-MOR and (▲) H-ZSM-12.

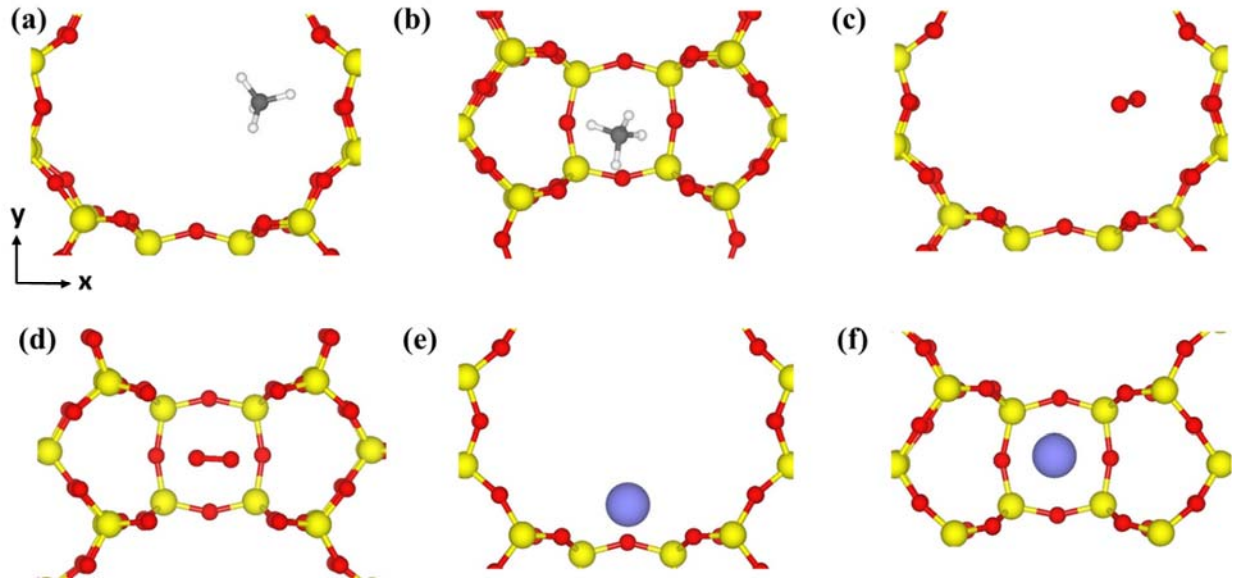

Figure 5. Most stable adsorption structure of: (a) methane in 12 MR channel, (b) methane in 8MR side pockets, (c) oxygen in 12 MR channel, (d) oxygen in 8 MR side pockets, (e) argon in 12 MR channel, and (f) argon in 8 MR side pockets of MOR. Key: Oxygen (●), silicon (●), carbon (●), hydrogen (○), and argon (●).

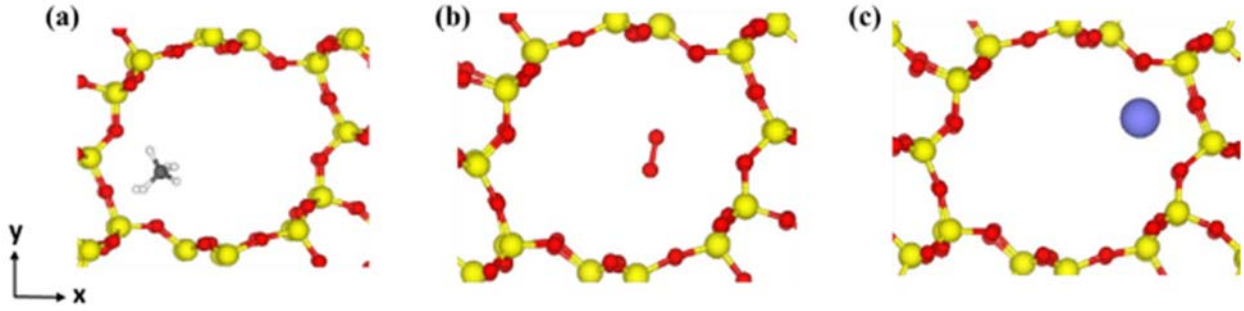

Figure 6: Most stable adsorption structure of (a) methane, (b) oxygen, and (c) argon in the 12 MR channels of ZSM-12. Key: Oxygen (●), silicon (●), carbon (●), argon (●), and hydrogen (○).